Geophysical Research Letters

RESEARCH LETTER
10.1029/2022GL100364

Key Points:

- Steady state measurements of hydrogen-water relative permeability
- Numerical history matching needed for extrapolation
- Strong hysteresis observed between drainage and imbibition

Supporting Information:

Supporting Information may be found in the online version of this article.

Correspondence to:

M. Lysyy,
Maksim.Lysyy@uib.no

Citation:

Lysyy, M., Føyen, T., Johannesen, E. B., Fernø, M., & Ersland, G. (2022). Hydrogen relative permeability hysteresis in underground storage. *Geophysical Research Letters*, *49*, e2022GL100364. https://doi.org/10.1029/2022GL100364

Received 8 JUL 2022
Accepted 29 AUG 2022

Hydrogen Relative Permeability Hysteresis in Underground Storage

Maksim Lysyy[1], Tore Føyen[2], Else Birkeland Johannesen[1], Martin Fernø[1], and Geir Ersland[1]

[1]Department of Physics and Technology, University of Bergen, Bergen, Norway, [2]SINTEF Industry, Trondheim, Norway

Abstract Implementation of the hydrogen economy for emission reduction will require storage facilities, and underground hydrogen storage (UHS) in porous media offers a readily available large-scale option. Lack of studies on multiphase hydrogen flow in porous media is one of the several barriers for accurate predictions of UHS. This paper reports, for the first time, measurements of hysteresis in hydrogen-water relative permeability in a sandstone core under shallow storage conditions. We use the steady state technique to measure primary drainage, imbibition and secondary drainage relative permeabilities, and extend laboratory measurements with numerical history matching and capillary pressure measurements to cover the whole mobile saturation range. We observe that gas and water relative permeabilities show strong hysteresis, and nitrogen as substitute for hydrogen in laboratory assessments should be used with care. Our results serve as calibrated input to field scale numerical modeling of hydrogen injection and withdrawal processes during porous media UHS.

Plain Language Summary Hydrogen storage facilities will need a ramp-up when the hydrogen share in the future energy mix increase. Large-scale hydrogen storage can be implemented in empty hydrocarbon fields or ground water reservoirs. Hydrogen storage in such media involve complex interactions with native rocks and fluids, and injection and withdrawal are typically described by flow functions. Relative permeability is one of the key flow functions that describe how easily hydrogen can flow through porous media in the presence of other fluids. In underground storage, hydrogen is cyclically injected and withdrawn multiple times, and its relative permeability may differ between these two processes, described as hysteresis. In this paper, we investigate hydrogen relative permeability in the laboratory and match with results from numerical simulations. We find that hydrogen relative permeability is different for injection and withdrawal and is also different from that of nitrogen. Our results are directly applicable in computer simulators that predict hydrogen storage efficiency.

1. Introduction

Hydrogen (H_2) will play a key role in low-carbon energy transitions, and it is vital to implement hydrogen storage technologies to enable its safe and economic use at industrial scale. Underground hydrogen storage (UHS) in porous media such as aquifers, depleted hydrocarbon fields, and coal seams has been proposed as widely available long-term and large-scale storage options (Iglauer et al., 2021; Muhammed et al., 2022). As for underground natural gas storage (UGS), UHS involves cyclic gas injection at peak supply (known as cushion gas) and withdrawal at peak demand (working gas). Despite the increasing attention to the topic worldwide, the fundamentals of multiphase hydrogen flow in porous media are still not well described. In particular, relative permeability hysteresis has not been addressed, although its impact has been previously assessed for UGS and CO_2 storage (Colonna et al., 1972; Juanes et al., 2006). The cyclic nature of the UHS suggests that distinct relative permeability functions must be implemented for hydrogen injection (drainage) and withdrawal (imbibition).

Relative permeability is a crucial input parameter for the UHS numerical modeling at field scale (Kanaani et al., 2022; Lysyy et al., 2021; Wang et al., 2022). Laboratory gas-water relative permeability curves often have low endpoint gas saturations (<65%) and relative permeabilities (<40%) due to the rock heterogeneity, capillary end effects, gravity segregation, and/or maximum experimental capillary pressure (Krevor et al., 2012; Muller, 2011). Numerical and/or analytical methods are therefore required to validate and extrapolate relative permeabilities in a wider saturation range.

Hydrogen-water relative permeability measurements are scarce in the open literature. Steady state drainage experiments resulted in low endpoint gas saturation (~60%) and relative permeability (~4%) (Yekta et al., 2018). The authors used experimental capillary pressure to analytically expand the relative permeability curves to higher

hydrogen saturations. However, their data set lacked numerical history matching. Unsteady state drainage measurements examined the effect of pressure, brine salinity, and rock type on hydrogen relative permeabilities (Rezaei et al., 2022). Their measurements were history matched but without extrapolation to higher gas saturations. None of the studies investigated relative permeability hysteresis. When used as input for field scale modeling studies, lack of numerical history matching and hysteresis may significantly impact the accuracy of modeling results.

We investigate hysteretic behavior in steady state hydrogen-water relative permeability during drainage, imbibition, and secondary drainage injections, aided by primary drainage capillary pressure measurements. The experimental measurements are numerically validated and history matched to derive relative permeabilities over the entire range of mobile gas saturations. Hydrogen primary drainage relative permeability is compared with nitrogen. Our results provide vital input with a direct impact on the USH modeling at field scale.

2. Materials and Methods

Steady state gas and water relative permeability (K_r) and porous plate capillary pressure (P_c) measurements were performed chronologically:

1. Primary drainage K_r with nitrogen (N_2),
2. Primary drainage K_r with hydrogen (H_2),
3. Primary drainage P_c and irreducible water saturation (S_{wirr}) establishment with N_2,
4. Imbibition K_r with H_2,
5. Secondary drainage K_r with H_2.

We used the same core sample for all experiments.

2.1. Materials

A Berea sandstone core sample was supplied by Kocurek Industries and analyzed for its key properties (Table S1 in Supporting Information S1). The porosity was measured by mass balance (brine) and $NaNO_3$ flooding, whereas the brine absolute permeability was determined based on the Darcy's law with four injection rates in the range of 0.15–0.60 ml/min. Brine was doped with cesium chloride CsCl (2.5 wt% NaCl/2.5 wt% CsCl) to enhance the brine *x*-ray adsorption, thereby improving the signal-to-noise ratio during in situ saturation monitoring.

A hydrophilic ceramic porous plate with 15 bar (gas-water) threshold pressure was provided by Soil Moisture and its properties were measured (Table S1 in Supporting Information S1). The porosity was determined by mass balance, whereas the absolute permeability was calculated based on induced water flux of 0.002 ml/min resulting from 1 bar differential pressure reported by the manufacturer.

2.2. Experimental Procedures

2.2.1. Relative Permeability Measurements

The K_r was measured by steady state method using eight injection steps with the total flow rate of 1 ml/min followed by a bump flood at 4 ml/min. The corresponding capillary numbers (N_{Ca}) were in the order of 10^{-8} (drainage) and 10^{-6} (imbibition), based on equations Equations S1, S2, and Table S4 in Supporting Information S1. Each injection step was terminated after differential pressure stabilization and injection of at least 15 pore volumes of total flow rate (Table S5 in Supporting Information S1). The experiments were run at 30 bar and 30°C, representing shallow storage conditions.

The experimental setup is a closed loop system where the fluids are fully recirculated (Figure S1 in Supporting Information S1). The core sample was wrapped in a 0.025 mm thick nickel foil to reduce hydrogen diffusion through the rubber sleeve in a vertically oriented biaxial core holder. Two Quizix pumps injected the gas and aqueous (brine) phases from the core holder top (drainage) or bottom (imbibition). A compensation pump maintained constant outlet pressure in the acoustic two-phase separator, where the effluent fluids were produced, measured, and circulated back to the injection pumps. The water saturation (S_w) profile was measured in situ using *x*-ray monitoring and calculated from the Beer-Lambert law (Equation S3 in Supporting Information S1), with the uncertainty ± 0.02 S_w units.

The closed loop setup enabled us to continuously monitor and detect potential hydrogen leaks. The volume changes of the compensation pump would indicate any impactful leakages in the system. The nickel foil proved to be a safe barrier between the core plug and the rubber sleeve. Hydrogen diffusion through the sleeve would easily be detected by the reduction in the confinement pressure that was continuously monitored. Small leakages are often inevitable when working with gases, but we accounted for any gas losses when interpreting the data from the two-phase separator. Overall, hydrogen can be safely used with conventional core flooding setup.

After primary drainage K_r experiments, the core sample was reestablished to $S_w = 1$, followed by P_c measurements toward S_{wirr}—an initial state prior to the imbibition K_r measurements. The secondary drainage K_r measurements started at the same core state established after the imbibition K_r measurements.

2.2.2. Capillary Pressure Measurements

Primary drainage P_c was measured with N_2 by porous plate method in a vertically oriented core holder and the core sample coupled in series with the porous plate. N_2 was injected from the top to the 100% brine-saturated core sample ($S_w = 1$), using four constant P_c steps in the range of 1.45–14 bar. The produced brine volume was recorded from a measuring cylinder, allowing to calculate the equilibrium S_w (i.e., termination of brine production) after each P_c step. The S_w after the final P_c step corresponded to S_{wirr} state, preparing the core sample for the imbibition K_r measurements.

2.3. Numerical History Matching

The commercial Sendra software was used to numerically verify the experimental performance and derive K_r and P_c (Prores, 2016). Sendra is a two-phase, one dimensional, black oil simulation tool for analysis of core scale experiments based on the Darcy's law and the continuity equation. The simulation model has 100 grid blocks in x-direction and hydrogen and water are immiscible. Hydrogen compressibility was neglected in the simulations because the compressibility factor is close to unity (<1.02) at experimental p-T conditions (Zhou & Zhou, 2001). Hydrogen thermodynamic properties (density and viscosity) were extracted from an open-source database (Linstrom & Mallard, 2001), which in turn used the equation of state and viscosity model derived specifically for hydrogen (Leachman et al., 2009; Muzny et al., 2013).

The initial solution was obtained through an automatic history matching of experimental measurements: Production data from two-phase separator, differential pressure, and S_w profiles from x-ray monitoring. The match quality was improved through a manual tuning of the LET model parameters for K_r and P_c (Lomeland et al., 2005, 2008):

Gas relative permeability:

$$K_{rg} = K^*_{rg} \cdot \frac{(1 - S_{wn})^{L_g}}{(1 - S_{wn})^{L_g} + E_g \cdot (S_{wn})^{T_g}} \tag{1}$$

Water relative permeability:

$$K_{rw} = K^*_{rw} \cdot \frac{(S_{wn})^{L_w}}{(S_{wn})^{L_w} + E_w \cdot (1 - S_{wn})^{T_w}} \tag{2}$$

where K^*_{rg} and K^*_{rw} are end points K_r at irreducible water saturation (S_{wirr}) and residual gas saturation (S_{gr}), respectively. L_g, E_g, T_g, L_w, E_w, and T_w are empirical fitting parameters. The normalized water saturation S_{wn} is defined as $S_{wn} = (S_w - S_{wirr})/(1 - S_{wirr} - S_{gr})$.

Primary drainage capillary pressure—simplified version for nonzero capillary threshold pressure:

$$P_c^{pd} = \frac{(P_{c,max} - P_{c,th}) \cdot (1 - S_{wx})^{L_s}}{(1 - S_{wx})^{L_s} + E_s \cdot (S_{wx})^{T_s}} + P_{c,th} \tag{3}$$

where $P_{c,max}$ and $P_{c,th}$ are maximum and threshold P_c, respectively, whereas L_s, E_s, and T_s are empirical fitting parameters. The normalized water saturation S_{wx} is defined as $S_{wx} = (S_w - S_{wirr})/(1 - S_{wirr})$.

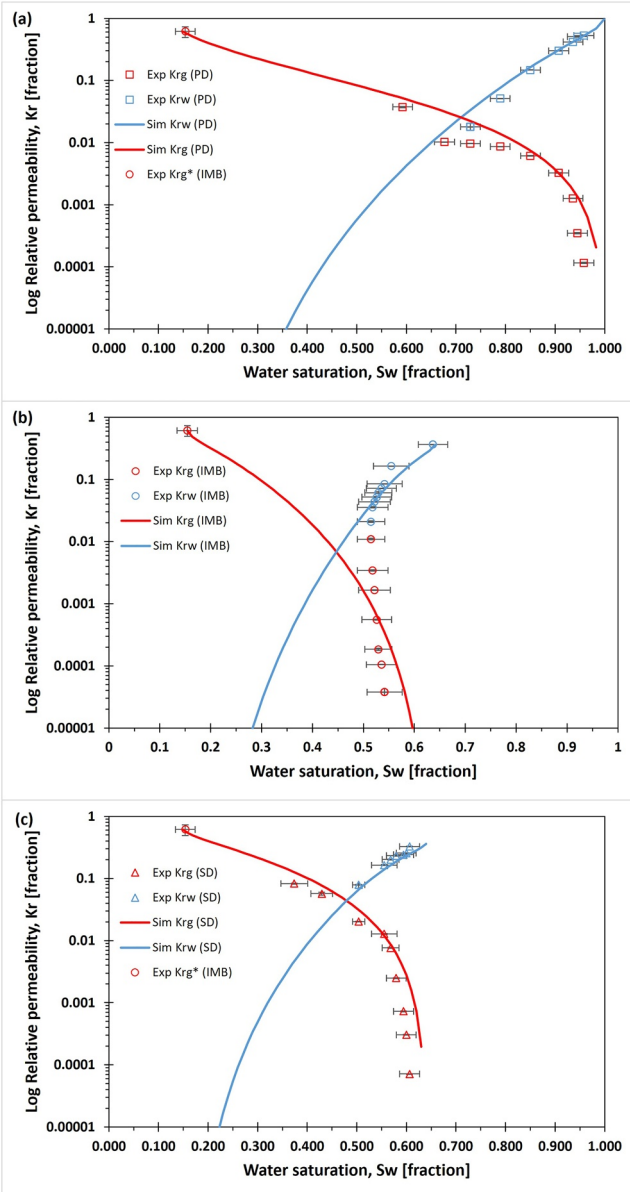

Figure 1. Experimental (Exp) and simulated (Sim) hydrogen-water relative permeabilities (K_r) on semilogarithmic scale for (a) primary drainage (PD), (b) imbibition (IMB), and (c) secondary drainage (SD). PD and SD K_r yield low endpoint values, and the endpoint K_{rg}^* at irreducible water saturation from IMB experiment is used to extrapolate K_r to low S_w region. The S_w values are calculated from *x*-ray scan for PD, whereas for IMB and SD the S_w are calculated as the average between *x*-ray scan and the two-phase separator production data. The K_r error bars represent the differential pressure uncertainty of ~2%, whereas the S_w error bars represent either the *x*-ray scan uncertainty of 0.02 S_w units (PD) or the uncertainty of the average S_w calculated from *x*-ray scan and two-phase separator (IMB and SD). Tabulated values are presented in Tables S6–S8, S10, and S11 in Supporting Information S1, respectively. A comparison between K_r is shown in Figure 2.

Imbibition and secondary drainage capillary pressure equations are presented in Equations S4 and S6 in Supporting Information S1.

3. Results and Discussion

3.1. Hydrogen-Water Relative Permeability

The hydrogen-water relative permeability was measured for primary drainage, imbibition, and secondary drainage injection processes (Figure 1). The endpoints were $K_{rg} = 0.04$ at $S_w = 0.59$ and $K_{rg} = 0.08$ at $S_w = 0.37$ after primary and secondary drainage, respectively. The low endpoints after primary and secondary drainage agreed with published K_r measurements in CO_2- and H_2-H_2O systems (Akbarabadi & Piri, 2013; Krevor et al., 2012; Yekta et al., 2018). The imbibition endpoints were $K_{rw} = 0.36$ at $S_w = 0.64$ (or $S_{gr} = 0.36$), within the expected range for Berea sandstones according to the Land trapping model with the trapping coefficients (C) between 1 and 1.407 and corresponding S_{gr} range of 0.35–0.42 (Krevor et al., 2012; Land, 1968; Ni et al., 2019).

The relative permeabilities curves were found directly from the stabilized differential pressure and saturation. Capillary end effects were evident (Figures S2c and S4c in Supporting Information S1), and the experimental measurements (Figures S2–S4 in Supporting Information S1) were history matched based on the LET model for relative permeability and capillary pressure (Tables 1 and 2). The primary and secondary drainage K_r were extrapolated for expected reservoir flows (lower S_w region), based on the $S_{wirr} = 0.15$ and history matched P_c from porous plate experiment and the endpoint $K_{rg}^* = 0.61$ from imbibition experiment. A minor deviation between measured (points) and simulated (solid lines) K_r curves (Figure 1) arise from the underlying assumptions on P_c gradients: Measured K_r assumed homogenous rock properties and zero capillary pressure, whereas the simulation incorporates a more realistic nonzero capillary pressure. The quality of the history matching was lower in the imbibition experiment (Figure 1b). Most of the hydrogen was produced from the core after the first injection step, with very little production in subsequent injection steps until bump flood (Figure S3b in Supporting Information S1). This behavior resembled a typical unsteady state experiment, which affected the simulator performance in a steady state mode. In general, the simulated K_r will better represent reservoir flow and should therefore be used as input for field scale simulations.

3.2. Hysteresis in Hydrogen-Water Relative Permeability

The relative permeability curves K_{rg} and K_{rw} showed strong hysteresis and hydrophilic preference, with the following primary drainage cross point values: $K_{rg} = K_{rw} = 0.025$ at $S_w = 0.71$ (Figure 2). Berea sandstones are originally strongly hydrophilic (Iglauer et al., 2015), but hydrogen systems become less hydrophilic with increasing pressure and organic acid concentration and decreasing temperature (Ali et al., 2021). The K_{rg} was higher for primary drainage than imbibition, whereas the secondary drainage K_{rg} was positioned between these two K_{rg}. Hysteretic K_{rg} behavior was consistent with previous gas-water K_r measurements and arise from residual gas trapping during imbibition (Akbarabadi & Piri, 2013; Ge et al., 2022; Oak et al., 1990; Peng, 2020; Ruprecht et al., 2014). The K_{rw} was lower for primary drainage than imbibition, in agreement with most studies and explained by contact angle hysteresis (Akbarabadi & Piri, 2013; Ge et al., 2022;

Table 1
Relative Permeability LET Model Parameters

	S_{wirr}	S_{gr}	K_{rg}^*	K_{rw}^*	L_w	E_w	T_w	L_g	E_g	T_g
Primary drainage H_2	0.15	0	0.61	1	7.5	2.95	0.52	1.6	6.0	0.9
Primary drainage N_2	0.15	0	0.73	1	6.5	3.9	0.8	2.2	1.5	0.7
Imbibition H_2	0.15	0.36	0.61	0.36	7.5	2.0	0.6	4.2	2.5	0.6
Secondary drainage H_2	0.15	0.36	0.61	0.36	5.2	2.0	0.7	1.88	2.1	0.7

Peng, 2020). Nonhysteretic K_{rw} behavior has also been reported in literature and attributed to reproducibility of drainage and imbibition injections in strongly hydrophilic systems (Oak et al., 1990; Ruprecht et al., 2014). Discrepancies in reported K_{rw} hysteresis can have a significant impact on the UHS modeling at field scale and must therefore be targeted in future studies.

3.3. Effect of Gas Type on Primary Drainage Relative Permeability

The primary drainage K_r gas-water measurements were repeated with nitrogen (N_2) and resulted in endpoint $K_{rg} = 0.06$ at $S_w = 0.59$, similar to H_2-H_2O system (Figure 3). The K_{rg} and K_{rw} curves shifted upward in the N_2-H_2O system, reflecting the impact of increased gas-water viscosity ratio (Jeong et al., 2017): N_2 is two times more viscous than H_2 at experimental conditions (Table S4 in Supporting Information S1). Note that difference in K_{rg} and K_{rw} is asymmetric, with a significantly greater increase in K_{rg} (~100% higher than in H_2 experiment) compared to K_{rw} (~50% higher than in H_2 experiment). We attribute this phenomenon to the combined effect of increased viscosity ratio and uncertainties in N_2 experiment.

Uncertainties in K_r (N_2) curves were mainly related to (a) nonconstant S_w distribution prior to first injection step (Figure S5c in Supporting Information S1), (b) too low water injection rate (1/10 of planed rate) during the second injection step (Table S5 in Supporting Information S1), and (c) missing measurement of endpoint K_{rg}^* (N_2). The endpoint K_{rg}^* (N_2) was set to 0.73 equal to the upper uncertainty limit of K_{rg}^* (H_2) because a higher K_{rg} was necessary to history match the N_2-experimental data. Note that history matching can yield several nonunique solutions, depending on the input parameters and matching strategy. Hence, the observed increased K_{rg} for the N_2-H_2O system reflects the uncertainty span of gas-water K_r in a Berea sandstone and may not represent an actual difference between K_r curves using N_2 and H_2. Although the use of analog fluids has previously been justified for Berea sandstones (Krevor et al., 2012), caution should be taken when using N_2 as a substitute for H_2 experimental measurements.

3.4. Field Scale Implications

Low experimental endpoint S_g^{max} and K_{rg} demonstrated the importance of numerical history matching. Strong hysteresis was observed both for K_{rg} and K_{rw}, and a full cycle of drainage and imbibition relative permeabilities must be implemented in future modeling studies for more accurate prediction of H_2 injection and withdrawal in the UHS.

Table 2
Capillary Pressure LET Model Parameters

	$P_{c,max}$ (kPa)	$P_{c,min}$ (kPa)	$P_{c,th}$ (kPa)	S_{wsi}	L_s	E_s	T_s	L_f	E_f	T_f
Primary drainage H_2	1,400		5.0		1	130.0	1	1	0.002	1
Primary drainage N_2	1,400		12.35		1	129.6	1	1	0.007	1
Imbibition H_2	1,400	−1,400	−0.1	0.45	1		1	1	120.0	1
Secondary drainage H_2	1,400	−0.001	−0.05	0.19	1		1	1	156.3	1
Porous plate N_2	1,400		1		1	450.0	1	1	3.5	1

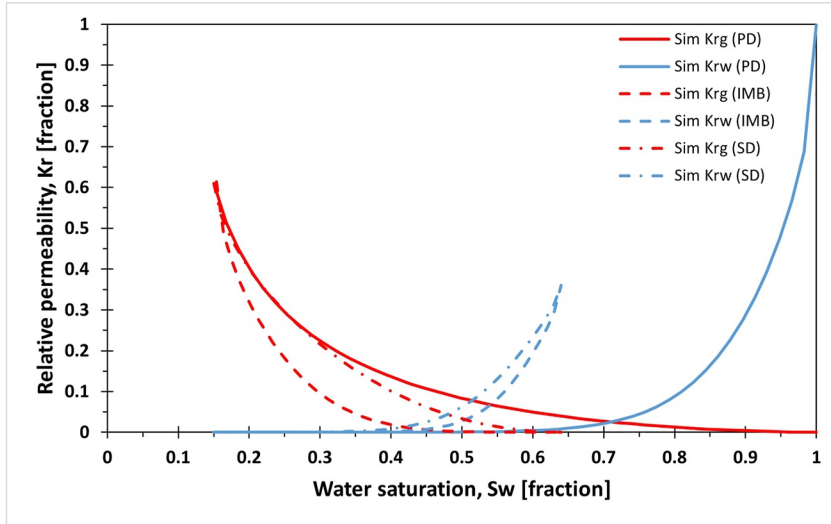

Figure 2. Hydrogen-water relative permeabilities show strong hysteresis both for hydrogen (K_{rg}) and water (K_{rw}).

Our K_r measurements are directly applicable for shallow sandstone aquifers with permeability in the order of ∼100 mD but can be used for deeper aquifers too. It was previously shown that K_r measurements for H_2 were independent of pressure-temperature conditions (Yekta et al., 2018). If omitting hysteresis for the sake of computational efficiency, imbibition K_r is most suitable for the UHS in depleted gas fields with an underlying aquifer. Drainage K_r models would better represent H_2 storage in aquifers.

Differences between primary drainage K_r for H_2 and N_2 has major implication over the choice of cushion gas. Higher K_{rw} for N_2-H_2O system will result in a more efficient water removal during N_2 injection relative to H_2, making N_2 a suitable cushion gas. Our conclusion correlates with contact angle measurements that indicate stronger N_2 wetting and, hence, better injectivity relative to H_2 (Al-Yaseri & Jha, 2021). During gas withdrawal, on the other hand, higher K_{rg} for N_2 will result in a more rapid N_2 flow relative to H_2, leading to an earlier N_2 breakthrough in the producing well. From the economic perspective, earlier N_2 breakthrough is undesired due to reduced H_2 purity in the withdrawn gas mixture. Note that the actual K_{rg} difference between H_2 and N_2 may be less than observed in our work due to methodological uncertainties. Both H_2 and N_2 K_r can be used in the UHS simulation studies as a part of sensitivity analysis.

4. Conclusions

We measured steady state hydrogen-water relative permeabilities in a Berea sandstone under shallow reservoir storage conditions. Three different relative permeability measurements were performed: Primary drainage, imbibition, and secondary drainage and were supported with porous plate capillary pressure measurements. We observed low endpoints for drainage curves, with hydrogen relative permeabilities and saturations less than 0.08 and 0.63, respectively. Numerical history matching was performed to extrapolate relative permeabilities to lower water saturations. Relative permeability curves showed strong hysteresis, both for hydrogen and water. Primary drainage relative permeability measurements were repeated with nitrogen, and relative permeabilities were higher than that of hydrogen due to the combined effect of increased viscosity ratio and methodological uncertainties. Our results have a direct and immediate implication for the impact of hysteresis on field scale numerical modeling in underground hydrogen storage.

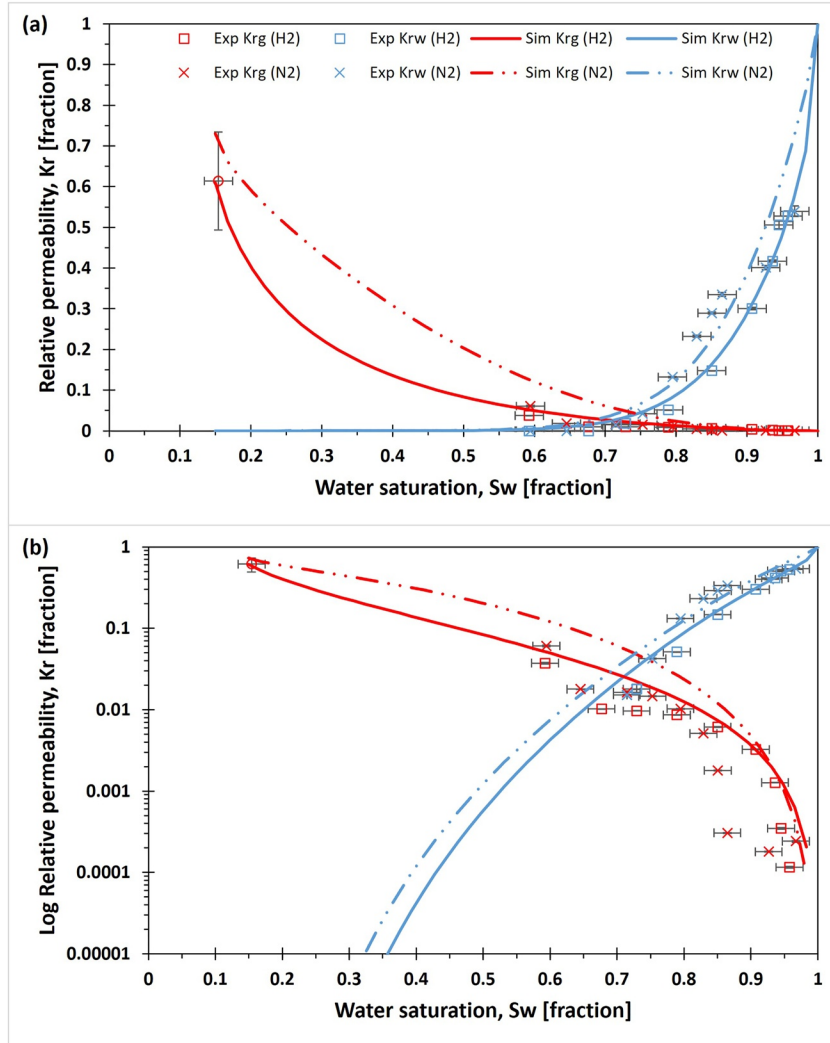

Figure 3. Hydrogen versus nitrogen primary drainage relative permeabilities, plotted in (a) linear and (b) semilogarithmic scales. Endpoint K_{rg} and S_w are similar for H_2 and N_2 measurements. K_{rg} and K_{rw} are higher for N_2, reflecting the combined effect of increased gas viscosity and methodological uncertainty. The endpoint K_{rg}^* at irreducible water saturation from H_2 imbibition experiment is used to extrapolate experimental K_{rg} (H_2) to low S_w region. The endpoint K_{rg}^* (N_2) at irreducible water saturation was not measured and is set to the upper uncertainty limit of the endpoint K_{rg}^* (H_2). Note that the K_{rg}^* from H_2 experiment represents a significant uncertainty (20%) due to small differential pressure (~4–8 mbar) caused by low hydrogen viscosity. Tabulated experimental and simulated values for N_2 experiment are presented in Tables S6 and S10 in Supporting Information S1, respectively.

Acknowledgments
The authors acknowledge the financial support from the Research Council of Norway under project *Hydrogen Storage in Subsurface Porous Media—Enabling Transition to Net-Zero Society* (project number 325457) and *Clean offshore energy by hydrogen storage in petroleum reservoirs* (project number 315804). The authors also acknowledge support from University of Bergen and the Petroleum Research School of Norway. Prores AS is acknowledged for granting the Sendra university license and SINTEF Industry is acknowledged for providing the access to the *x*-ray flow rig in Trondheim. Kristina Smirnova from Resbridge AS is acknowledged for valuable discussions on numerical history matching.

Data Availability Statement

Data sets from relative permeability measurements are uploaded to http://dx.doi.org/10.17632/rfhf7wjydn.1, an open-source online data repository hosted by Mendeley Data. The core scale simulator Sendra developed by Prores AS is available at https://www.prores.no/solution/sendra.

References

Akbarabadi, M., & Piri, M. (2013). Relative permeability hysteresis and capillary trapping characteristics of supercritical CO_2/brine systems: An experimental study at reservoir conditions. *Advances in Water Resources*, *52*, 190–206. https://doi.org/10.1016/j.advwatres.2012.06.014

Ali, M., Yekeen, N., Pal, N., Keshavarz, A., Iglauer, S., & Hoteit, H. (2021). Influence of pressure, temperature and organic surface concentration on hydrogen wettability of caprock; implications for hydrogen geo-storage. *Energy Reports*, *7*, 5988–5996. https://doi.org/10.1016/j.egyr.2021.09.016

Al-Yaseri, A., & Jha, N. K. (2021). On hydrogen wettability of basaltic rock. *Journal of Petroleum Science and Engineering*, *200*, 108387. https://doi.org/10.1016/j.petrol.2021.108387

Colonna, J., Brissaud, F., & Millet, J. L. (1972). Evolution of capillarity and relative permeability hysteresis. *Society of Petroleum Engineers Journal*, *12*(1), 28–38. https://doi.org/10.2118/2941-Pa

Ge, J., Zhang, X., Liu, J., Almutairi, A., & Le-Hussain, F. (2022). Influence of capillary pressure boundary conditions and hysteresis on CO_2-water relative permeability. *Fuel*, *321*, 124132. https://doi.org/10.1016/j.fuel.2022.124132

Iglauer, S., Abid, H., Al-Yaseri, A., & Keshavarz, A. (2021). Hydrogen adsorption on sub-bituminous coal: Implications for hydrogen geo-storage. *Geophysical Research Letters*, *48*(10), e2021GL092976. https://doi.org/10.1029/2021GL092976

Iglauer, S., Pentland, C. H., & Busch, A. (2015). CO_2 wettability of seal and reservoir rocks and the implications for carbon geo-sequestration. *Water Resources Research*, *51*(1), 729–774. https://doi.org/10.1002/2014wr015553

Jeong, G. S., Lee, J., Ki, S., Huh, D. G., & Park, C. H. (2017). Effects of viscosity ratio, interfacial tension and flow rate on hysteric relative permeability of CO_2/brine systems. *Energy*, *133*, 62–69. https://doi.org/10.1016/j.energy.2017.05.138

Juanes, R., Spiteri, E. J., Orr, F. M., & Blunt, M. J. (2006). Impact of relative permeability hysteresis on geological CO_2 storage. *Water Resources Research*, *42*(12), W12418. https://doi.org/10.1029/2005wr004806

Kanaani, M., Sedaee, B., & Asadian-Pakfar, M. (2022). Role of cushion gas on underground hydrogen storage in depleted oil reservoirs. *Journal of Energy Storage*, *45*, 103783. https://doi.org/10.1016/j.est.2021.103783

Krevor, S. C. M., Pini, R., Zuo, L., & Benson, S. M. (2012). Relative permeability and trapping of CO_2 and water in sandstone rocks at reservoir conditions. *Water Resources Research*, *48*(2), W02532. https://doi.org/10.1029/2011wr010859

Land, C. S. (1968). Calculation of imbibition relative permeability for two and three-phase flow from rock properties. *Society of Petroleum Engineers Journal*, *8*(2), 149–156. https://doi.org/10.2118/1942-Pa

Leachman, J. W., Jacobsen, R. T., Penoncello, S. G., & Lemmon, E. W. (2009). Fundamental equations of state for parahydrogen, normal hydrogen, and orthohydrogen. *Journal of Physical and Chemical Reference Data*, *38*(3), 721–748. https://doi.org/10.1063/1.3160306

Linstrom, P. J., & Mallard, W. G. (2001). The NIST chemistry WebBook: A chemical data resource on the internet. *Journal of Chemical and Engineering Data*, *46*(5), 1059–1063. https://doi.org/10.1021/je000236i

Lomeland, F., Ebeltoft, E., & Thomas, W. H. (2005). A new versatile relative permeability correlation. In *The International Symposium of the Society of Core Analysts* (Vol. 112).

Lomeland, F., Ebeltoft, E., & Thomas, W. H. (2008). A new versatile capillary pressure correlation. In *The International Symposium of the Society of Core Analysts* (Vol. 29).

Lysyy, M., Ferno, M., & Ersland, G. (2021). Seasonal hydrogen storage in a depleted oil and gas field. *International Journal of Hydrogen Energy*, *46*(49), 25160–25174. https://doi.org/10.1016/j.ijhydene.2021.05.030

Muhammed, N. S., Haq, B., Al Shehri, D., Al-Ahmed, A., Rahman, M. M., & Zaman, E. (2022). A review on underground hydrogen storage: Insight into geological sites, influencing factors and future outlook. *Energy Reports*, *8*, 461–499. https://doi.org/10.1016/j.egyr.2021.12.002

Muller, N. (2011). Supercritical CO_2-brine relative permeability experiments in reservoir rocks-literature review and recommendations. *Transport in Porous Media*, *87*(2), 367–383. https://doi.org/10.1007/s11242-010-9689-2

Muzny, C. D., Huber, M. L., & Kazakov, A. F. (2013). Correlation for the viscosity of normal hydrogen obtained from symbolic regression. *Journal of Chemical and Engineering Data*, *58*(4), 969–979. https://doi.org/10.1021/je301273j

Ni, H., Boon, M., Garing, C., & Benson, S. M. (2019). Predicting CO_2 residual trapping ability based on experimental petrophysical properties for different sandstone types. *International Journal of Greenhouse Gas Control*, *86*, 158–176. https://doi.org/10.1016/j.ijggc.2019.04.024

Oak, M. J., Baker, L. E., & Thomas, D. C. (1990). Three-phase relative permeability of Berea sandstone. *Journal of Petroleum Technology*, *42*(8), 1054–1061. https://doi.org/10.2118/17370-PA

Peng, S. (2020). Gas-water relative permeability of unconventional reservoir rocks: Hysteresis and influence on production after shut-in. *Journal of Natural Gas Science and Engineering*, *82*, 103511. https://doi.org/10.1016/j.jngse.2020.103511

Prores. (2016). Sendra (Version 2016.2). Retrieved from https://www.prores.no/solution/sendra

Rezaei, A., Hassanpouryouzband, A., Molnar, I., Derikvand, Z., Haszeldine, R. S., & Edlmann, K. (2022). Relative permeability of hydrogen and aqueous brines in sandstones and carbonates at reservoir conditions. *Geophysical Research Letters*, *49*(12), e2022GL099433. https://doi.org/10.1029/2022GL099433

Ruprecht, C., Pini, R., Falta, R., Benson, S., & Murdoch, L. (2014). Hysteretic trapping and relative permeability of CO_2 in sandstone at reservoir conditions. *International Journal of Greenhouse Gas Control*, *27*, 15–27. https://doi.org/10.1016/j.ijggc.2014.05.003

Wang, G., Pickup, G., Sorbie, K., & Mackay, E. (2022). Scaling analysis of hydrogen flow with carbon dioxide cushion gas in subsurface heterogeneous porous media. *International Journal of Hydrogen Energy*, *47*(3), 1752–1764. https://doi.org/10.1016/j.ijhydene.2021.10.224

Yekta, A. E., Manceau, J. C., Gaboreau, S., Pichavant, M., & Audigane, P. (2018). Determination of hydrogen-water relative permeability and capillary pressure in sandstone: Application to underground hydrogen injection in sedimentary formations. *Transport in Porous Media*, *122*(2), 333–356. https://doi.org/10.1007/s11242-018-1004-7

Zhou, L., & Zhou, Y. P. (2001). Determination of compressibility factor and fugacity coefficient of hydrogen in studies of adsorptive storage. *International Journal of Hydrogen Energy*, *26*(6), 597–601. https://doi.org/10.1016/S0360-3199(00)00123-3

References From the Supporting Information

Foyen, T., Alcorn, Z. P., Ferno, M. A., Barrabino, A., & Holt, T. (2021). CO_2 mobility reduction using foam stabilized by CO_2- and water-soluble surfactants. *Journal of Petroleum Science and Engineering*, *196*, 107651. https://doi.org/10.1016/j.petrol.2020.107651

Massoudi, R., & King, A. D. (1974). Effect of pressure on surface-tension of water - adsorption of low-molecular weight gases on water at 25 degrees. *Journal of Physical Chemistry*, *78*(22), 2262–2266. https://doi.org/10.1021/j100615a017